Detection of emphysema in rat lungs by using magnetic resonance measurements of ^{3}He diffusion

X. Josette Chen*†, Laurence W. Hedlund*, Harald E. Möller‡, Mark S. Chawla*, Robert R. Maronpot§, and G. Allan Johnson*¶

*Center for In Vivo Microscopy, Duke University Medical Center, Durham, North Carolina 27710; ‡Institut für Physikalische Chemie, Westfälische Wilhelms-Universität, D-48149 Münster, Germany; and §National Institute of Environmental Health Sciences, Division of Chemical Pathology and Toxicology, Research Triangle Park, North Carolina 27709

Communicated by William Happer, Princeton University, Princeton, NJ, July 27, 2000 (received for review November 29, 1999)

Emphysema is a pulmonary disease characterized by alveolar wall destruction, resulting in enlargement of gas exchange spaces without fibrosis. This condition is a part of chronic obstructive pulmonary disease (COPD), which causes 3.5% of deaths worldwide [Anonymous (1990) *World Health Stat. Q. Special*, 1–51] and contributes greatly to the global burden of disease [Murray, C. J. & Lopez, A. D. (1996) *Science* 274, 740–743]. Alveolar regeneration has been shown in animal models and could have potential for clinical treatment of early-stage emphysema. However, current techniques for detection of emphysema are not sensitive at the initial stages. Early-stage human panacinar emphysema is modeled in elastase-treated animals. Here, we provide an *in vivo* imaging method for differentiating normal and emphysematous rat lungs by measuring the apparent diffusion coefficient (ADC) of hyperpolarized ^{3}He by using magnetic resonance imaging. These data show that the ADC is significantly larger in elastase-treated rats, indicating alveolar expansion. Whereas these rats were clinically asymptomatic, conventional histology confirmed presence of injury. Our results indicate that measurement of the hyperpolarized ^{3}He ADC can be a valuable research tool and has potential application in the clinical setting.

Conventional MRI (1) uses the water hydrogen nuclei present in the body as a signal source. The volume of the lungs comprises only 10% tissue, making MRI in this organ very difficult. By applying the same magnetic resonance (MR) principles to laser-polarized [also called "hyperpolarized" (HP)] noble gases (2), a technique was developed that allowed direct imaging of the airways in the lungs (3). Initial success of this technique with clinical pulmonary disease has been shown by imaging the absence or presence of gas (density imaging), thus showing ventilation defects in the lung (4, 5). However, these studies were in patients with advanced stages of pulmonary disease, where alveolar wall destruction led to obstruction of gas flow (6). In the elastase-induced model of emphysema used here, only the enlargement of the distal air spaces (i.e., alveolar ducts and alveoli) is present (7, 8). It may be difficult for gas density imaging to differentiate between healthy distal air spaces and enlarged air spaces, because the amount of gas ventilated to the distal spaces in each situation is similar, and the size of individual alveolar clusters is beyond the current resolution limit. Another technique needs to be explored to measure emphysema in the early stages.

We have previously shown that the diffusion of HP gas is affected by its structural environment (9). The diffusion coefficient of HP gas was measured by using a magnetic resonance technique with bipolar pulsed gradients (10). The effect of the gradients is to label the nuclei so that the bulk diffusive motion can be tracked through imaging. In the guinea pig lung, the ^{3}He apparent diffusion coefficient in the distal air spaces was reduced 10-fold from the free diffusion coefficient because of interactions with airway structure and air molecules. In this study, we test the sensitivity of the ^{3}He apparent diffusion coefficient (ADC) to detect altered lung structure by measuring it in emphysematous and control rats.

Materials and Methods

Hyperpolarized Gas Production. ^{3}He was polarized by spin-exchange with laser-polarized rubidium (11). A prototype polarizer (IGI.9600.He, Magnetic Imaging Technologies, Durham, NC) was used to provide ≈1500 cm^3 of gas with a nuclear polarization of 30%–40% in 8 h. More details of this polarization technique may be found in refs. 12 and 13. The gas was transferred to a double-chambered Plexiglas vessel used to supply HP ^{3}He to the ventilator. The flexible inner chamber [1.6-liter Tedlar bag (Jensen Inert, Coral Springs, FL)] was evacuated to prevent O_2 contamination and then filled with HP gas by direct connection to the high-pressure glass cell. The transfer system was set in-line with the bore of the imaging magnet at a distance of ≈1 m and then connected to the breathing valve. The flow of the HP gas to the ventilator was regulated by constant ^{4}He pressure in the outer chamber.

Animal Preparation. To induce emphysema, adult male Fischer rats were first anesthetized with methohexital and perorally intubated. Then, porcine elastase dissolved in 0.2 ml of saline was endotracheally instilled (75 units/100 g body weight; Elastin Products, St. Louis) (8) (n = 6). Control rats (n = 6) were instilled with an equivalent volume of saline. All of the rats were imaged 4 wk after treatment. Experiments occurred in a pairwise fashion, with a control rat and an elastase-treated rat imaged on the same day (except for one of each treatment). To permit delivery of gas, an airway was established by peroral intubation with a 14-gauge intracatheter (Sherwood Medical Industries, St. Louis), and a gas-tight seal was established with two 3-0 silk ligatures tied around the trachea. ECG was recorded continuously from pediatric electrodes attached to the foot pads, a rectal thermistor monitored temperature, and a solid-state pressure transducer on the breathing valve monitored airway pressure.

Gas Delivery. HP gas was delivered to the live anesthetized rats via a custom-built MR-compatible pressure ventilator (14). The

Abbreviations: MR, magnetic resonance; HP, hyperpolarized; ADC, apparent diffusion coefficient; EEV, end expiratory volume; HB, held breath; H&E, hematoxylin-eosin.

†Present address: Sunnybrook & Women's College Health Sciences Center, Toronto, ON, Canada M5N 3M5.

¶To whom reprint requests should be addressed: C/O Elaine G. Fitzsimons, Center for *In Vivo* Microscopy, Duke University Medical Center, Box 3302, Durham, NC 27710. E-mail: egf@orion.mc.duke.edu.

The publication costs of this article were defrayed in part by page charge payment. This article must therefore be hereby marked "*advertisement*" in accordance with 18 U.S.C. §1734 solely to indicate this fact.

ventilator comprises pneumatic valves that are computer controlled with a TIO-10 digital board and LABVIEW software (National Instruments, Austin, TX). The ventilator computer provided the trigger for the MR imaging system. The ADC was measured in both groups of rats at two extreme lung volumes: functional residual capacity or end expiratory volume (EEV) and held breath (HB). Hence, the breathing rate was set at 60 breaths per minute, and two breathing methods were used: (*i*) held breath, an inspiration period of 250 ms, followed by a held breath period of 440 ms, and finally an expiration period of 310 ms; and (*ii*) end expiration, an inspiration period of 250 ms, followed by a held breath period of 60 ms, and finally an expiration period of 690 ms. A constant tidal volume (2 cm^3) was supplied for each breath consisting of 27% O_2, 2.5%–3.5% isoflurane (Aerrane; Ohmeda Caribe, Guayama, PR), and the balance HP ^{3}He.

Diffusion Imaging. MRI was performed on a 2.0 T, 30-cm-bore magnet (Oxford) with shielded gradients (180 mT/m) controlled by a Signa console (General Electric). A dual-frequency, 7-cm-diameter birdcage rf coil was used at 85.5 MHz and 65.1 MHz for ^{1}H and ^{3}He, respectively. The animal was placed in the prone position in the rf coil. Coronal and axial ^{1}H images were acquired before ^{3}He imaging to confirm proper location of the thorax in the coil and magnet. A 5-mm-thick axial slice was chosen to encompass the right diaphragmatic lobe and the left lobe (between the apex of the heart and the dome of the diaphragm).

Diffusion weighting was accomplished by using a modified projection-encoding sequence (9). Bipolar gradients were applied in a direction perpendicular to the long axis of the trachea before acquisition of the free induction decay. A series of six axial images was acquired by fixing the diffusion times ($\Delta = 1$ ms and $\delta = 0.5$ ms; ref. 9) and varying the gradient strengths (diffusion weighting ranging from 0 to 7.2 s/cm^2) such that the image intensity varied exponentially across the series. Relevant MR parameters were as follows: repetition time 10 ms, effective echo time 2.2 ms, flip angle 20°, field of view 40 mm, acquisition matrix 128 × 128, and slice thickness 5 mm. The acquisition of each image was accomplished over 25 breaths in a period of 25 s. Imaging occurred in the middle 400 ms of either HB or EEV periods.

Histology. After *in vivo* imaging, the rats were killed by anesthetic overdose, and the lungs were fixed by instilling a buffered solution of 2% gluteraldehyde/10% formalin at 25-cm H_2O intratracheal pressure (equivalent to total lung capacity). After 30 min of fixation, the trachea, lungs, and heart were excised en-block and stored in 10% formalin. Axially cut samples (7 μm thick) of both lower lobes, approximating the MR imaging plane, were processed for conventional hematoxylin-eosin (H&E) staining.

Data Analysis. All data analysis was accomplished by using MATLAB (MathWorks, Natick, MA). ADC maps were calculated by fitting a series of images on a pixel-by-pixel basis to an exponential decaying to a noise floor by using a nonlinear least-squares fitting technique (Gauss-Newton).

Statistical comparisons of lung volumes within a group were accomplished with paired *t* tests, and independent *t* tests were used between groups.

The method of measuring the mean linear intercept was semiautomated, based on a technique first proposed by Dunnill (15). The middle third (dorsal to ventral) of the axial slice was magnified ×54 (BX50, Olympus) and digitized. A binary image was manually formed with air spaces corresponding to 1 and lung tissue structure corresponding to 0 (Adobe Photoshop). About 50,000 lines were digitally overlaid on the sections, and intercepts with alveolar walls were automatically counted (minimum 35,000 per section). The mean linear intercept, *Lm*, was calculated according to the formula, $Lm = L/(X \times m)$, where L is the total length of all of the overlaid lines, X is the magnification factor, and m is the sum of all of the intercepts. The algorithm accounted for large blood vessels and large air spaces.

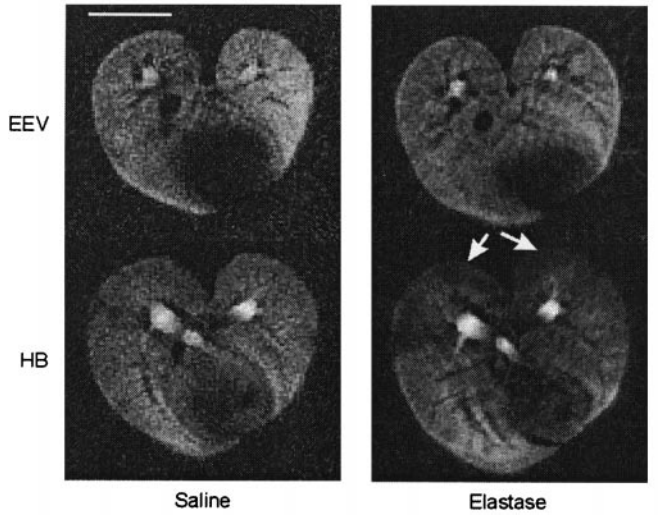

Fig. 1. Gas density images of representative animals from the control and elastase-treated groups at held breath and end expiratory volume. The arrows indicate lower signal intensity in the dorsal region. Bar = 10 mm.

Results and Discussion

Fig. 1 shows images of ^{3}He gas density (i.e., no applied diffusion pulses) in the lungs of representative animals from both groups at EEV and HB. Qualitatively, the cross-sectional area of the lung in the elastase-treated rat is larger than in the control rat at both lung volumes. In addition, there is lower signal in the dorsal region as compared with the rest of the image (indicated by arrows) of the elastase-treated rat at HB; the signal decrease is probably due to reduced ventilation to this section of the lung. These trends were noted in virtually all animals imaged. However, both of these observations are very subtle and indicate that gas density imaging may not be the appropriate method for detection of early stages of emphysema, unlike what has been shown in advanced-stage emphysematous patients (4, 5). Consequently, we used a more quantitative approach.

An ADC map (not shown) was calculated from the diffusion-weighted images. From the map, an ADC histogram was derived. Because elastase predominately affects the distal spaces, the diffusion coefficients from the large airways were excluded from consideration. Fig. 2 shows ADC histograms of the distal spaces of representative animals from each group. Table 1 shows all of the ADC averages from both groups at both respiratory volumes. These values are reduced from the free diffusion coefficient of ^{3}He in air (0.86 cm^2/s) because the diffusion is physically restricted. The distal air space dimensions are on the order of 0.0162 cm (16), which are smaller than the distance ^{3}He in air diffuses during our measurement ($l = \sqrt{(2D\Delta)} = 0.042$ cm). The larger histogram from the elastase-induced lung than the control lung corresponds to the larger cross-sectional area in the elastase lung, as mentioned above. To standardize an area throughout the center of the lung, the diffusion coefficients from the middle third of the axial image (dorsal to ventral) were averaged. No significant differences in the ADC were observed comparing right diaphragmatic and left lobes. The analysis of the data described in Table 1 showed that (*i*) the mean diffusion coefficient at HB was significantly greater than at EEV in the saline group ($P < 0.01$) and the elastase group ($P < 0.001$), (*ii*) the mean of the EEV distribution in the saline-treated lung was

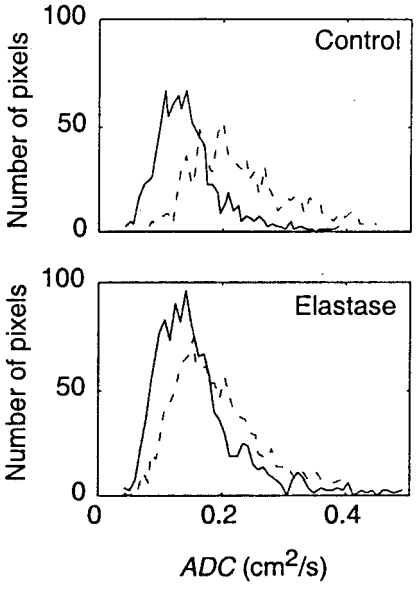

Fig. 2. Histograms of diffusion coefficients from the combined middle thirds (dorsal to ventral) of the right and left lung. Representative animals are shown from the control and elastase-treated groups at end expiratory volume (solid line) and held breath (dashed line).

significantly less than in the elastase-treated lung ($P < 0.01$), and (*iii*) the means of both groups at HB were not significantly different ($P > 0.20$).

The increase in the ADC from EEV to HB is expected because the alveolar dimensions increase with increasing tidal volume (17), hence the gas experiences less restriction to diffusion. The increased mean ADC at EEV in the elastase group as compared with the saline group implies that the distal air space volume is larger in the elastase group. This increase is anticipated in the emphysema model, because the EEV increases because of decreased elastic recoil (18, 19). It is difficult to comment on the lack of significant difference between the HB diffusion coefficients for both groups of animals because we used a pressure ventilator, which does not guarantee an equal tidal volume delivered to both sets of animals.

After *in vivo* imaging, the lungs were processed for conventional histology (see *Materials and Methods*). Examples of H&E sections shown in Fig. 3 demonstrate degradation of the alveolar walls, leading to larger airspaces in the elastase group, as expected. These H&E sections were analyzed by calculating the mean linear intercept (15, 20) (*Lm*), a method used to estimate air space size. Similar to the diffusion coefficient analysis, *Lm* was calculated in the middle third of the lung. Again, no

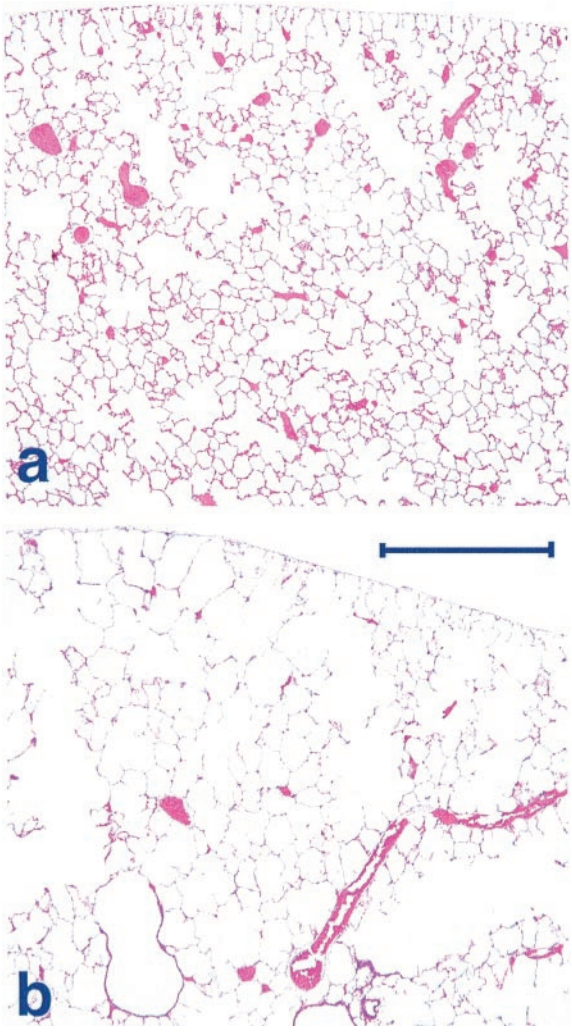

Fig. 3. Representative H&E sections from (*a*) the control group and (*b*) the elastase group. Bar = 1 mm.

significant difference was found between the right and left lobes. The *Lm* averaged from all of the control lungs was found to be 76.5 ± 1.9 μm (mean ± SEM). In comparison with the average of the elastase group, the *Lm* increased 27% to 97.3 ± 3.8 μm, confirming the enlargement of distal air spaces with elastase treatment. A direct comparison between *Lm* and the *in vivo* diffusion coefficient data was not possible due to a difference between the fixation volumes and *in vivo* tidal volumes. By

Table 1. The average ADC from the middle third (dorsal to ventral) of the lungs with the SD of the distribution in brackets for each of the rats studied

	Saline		Elastase	
	EEV ADC, cm²/s	HB ADC, cm²/s	EEV ADC, cm²/s	HB ADC, cm²/s
	0.14 (0.05)	0.34 (0.14)	0.19 (0.08)	0.24 (0.10)
	0.15 (0.06)	0.19 (0.10)	0.17 (0.07)	0.21 (0.08)
	0.13 (0.05)	0.23 (0.09)	0.18 (0.07)	0.22 (0.08)
	0.14 (0.05)	0.23 (0.08)	0.16 (0.07)	0.19 (0.07)
	0.10 (0.04)	0.20 (0.08)	0.15 (0.06)	0.18 (0.07)
*	0.15 (0.05)	0.22 (0.08)	0.16 (0.06)	0.21 (0.08)
Average	0.14 ± 0.02	0.24 ± 0.05	0.17 ± 0.02	0.21 ± 0.02

*These two animals were not done on the same day.
The average and SD from averaging of each are shown at the bottom of the table.

focusing future work on controlling the fixation volume, such that direct comparisons can be made between the two modalities, it is possible that the ADC could be used to deduce an absolute measure of air space size in the lung (9, 21).

HP gas imaging of lung air spaces by using gas density techniques appears promising for localization of defects in gas flow (4, 5). However, for more subtle injuries, measurement of the gas diffusion coefficient may be more appropriate, as we have shown in these results. Furthermore, the *in vivo* nature of the technique makes longitudinal studies possible. Hence, air space changes resulting from progression of disease or experimental treatments (19, 22) can be followed. Another direction for investigation is to calibrate the ADC by performing studies in phantoms with known dimensions (23–25). Thus, it may be possible to indirectly measure airway diameter even if the imaging resolution is insufficient to delineate alveolar clusters directly.

A competing method of measuring airway dimension is a nonradiographic technique using aerosol probes (26). However, unlike the present study, the aerosol method cannot be spatially localized. High-resolution computed tomography (HRCT) is the best-recognized clinical technique for detection of mild emphysema (27). However, in addition to the ionizing radiation imparted to the patient, HRCT does little to alter prognosis because identification is not early enough (28). With the possibility of even earlier detection, ADC mapping of HP ^{3}He has the potential to open up new research directions in the study and management of emphysema, especially with new understanding of the progress of emphysema (29) and development of potential new therapies (19, 22).

This work represents a demonstration of HP gas imaging as an indicator of disease in a controlled animal model. We have shown that the ADC measured *in vivo* is sensitive to structural changes in the lung. We estimate these changes correspond to about 20 μm, as measured by conventional histology. ADC imaging is sensitive to subtle changes in underlying microstructure without the need for comparable resolution. This technique of measuring the diffusion coefficient may be transferable to the clinical arena by acquiring fewer images for diffusion calculations, compensating for the larger human lung capacities (B. T. Saam, D. A. Yablonskiy, D. S. Gierada, J. D. Cooper & M. S. Conradi, unpublished work; and M. Salerno, J. R. Brookeman, E. E. de Lange, J. Knight-Scott & J. P. Mugler, unpublished work). An immediate challenge will be to find the changes in diffusion that indicate early onset of emphysema in the human. Additionally, the *in vivo* nature of this technique may provide a tool to investigate the impact of airborne pollutants (e.g., ozone or diesel exhaust) in experimental emphysematous lung. ADC imaging of HP ^{3}He would also be applicable to other pulmonary diseases affecting airway caliber (e.g., asthma, bronchiolitis obliterans, and bullous disease). We believe the concept of HP gas ADC measurement will contribute greatly to the scope of pulmonary studies of airway diseases in both the research and clinical arenas.

We thank C. Ted Wheeler for animal preparation, Dr. David M. Delong for assistance with statistics, and Elaine G. Fitzsimons for editorial assistance. This work was supported by the National Institutes of Health/National Heart, Lung, and Blood Institute (RO1 HL 55348) and National Institutes of Health/National Center for Research Resource (P41 RR05959). M.S.C. and H.E.M. acknowledge fellowships from the Whitaker Foundation and Deutsche Forschungsgemeinschaft (Mo 588/3-1), respectively.

1. Lauterbur, P. C. (1973) *Nature (London)* **242,** 190–191.
2. Happer, W., Miron, E., Schaefer, S., Schreiber, D., Wijngaarden, W. & Zeng, X. (1984) *Phys. Rev. A* **29,** 3092–3110.
3. Albert, M. S., Cates, G. D., Driehuys, B., Happer, W., Saam, B., Springer, C. S., Jr., & Wishnia, A. (1994) *Nature (London)* **370,** 199–201.
4. de Lange, E. E., Mugler, J. P., 3rd, Brookeman, J. R., Knight-Scott, J., Truwit, J. D., Teates, C. D., Daniel, T. M., Bogorad, P. L. & Cates, G. D. (1999) *Radiology* **210,** 851–857.
5. Kauczor, H. U., Ebert, M., Kreitner, K. F., Nilgens, H., Surkau, R., Heil, W., Hofmann, D., Otten, E. W. & Thelen, M. (1997) *J. Magn. Reson. Imaging* **7,** 538–543.
6. Takasugi, J. E. & Godwin, J. D. (1998) *Radiol. Clin. North. Am.* **36,** 29–55.
7. Kuhn, C. & Tavassoli, F. (1976) *Lab. Invest.* **34,** 2–9.
8. Busch, R. H., Lauhala, K. E., Loscutoff, S. M. & McDonald, K. E. (1984) *Environ. Res.* **33,** 497–513.
9. Chen, X. J., Möller, H. E., Chawla, M. S., Cofer, G. P., Driehuys, B., Hedlund, L. W. & Johnson, G. A. (1999) *Magn. Reson. Med.* **42,** 721–728.
10. Stejskal, E. O. & Tanner, J. E. (1965) *J. Chem. Phys.* **42,** 288.
11. Chupp, T., Wagshul, M., Coulter, K., McDonald, A. & Happer, W. (1987) *Phys. Rev. C* **36,** 2244–2251.
12. Middleton, H., Black, R., Saam, B., Cates, G., Cofer, G., Guenther, B., Happer, W., Hedlund, L., Johnson, G., Juvan, K. & Swartz, J. (1995) *Magn. Reson. Med.* **33,** 271–275.
13. Chen, X. J., Chawla, M. S., Hedlund, L. W., Möller, H. E., MacFall, J. R. & Johnson, G. A. (1998) *Magn. Reson. Med.* **39,** 79–84.
14. Hedlund, L. W., Cofer, G. P., Owen, S. J. & Johnson, G. A. (2000) *Magn. Reson. Imaging,* in press.
15. Dunnill, M. S. (1962) *Thorax* **17,** 320–328.
16. Kliment, V. (1973) *Folio Morphologica* **21,** 59–64.
17. Milic-Emili, J. (1977) in *Regional Differences in the Lung*, ed. West, J. B. (Academic, New York), pp. 172–173.
18. Yokoyama, E., Nambu, Z., Uchiyama, I. & Kyono, H. (1987) *Environ. Res.* **42,** 340–352.
19. Massaro, G. D. & Massaro, D. (1997) *Nat. Med.* **3,** 675–677.
20. Tomkeieff, S. I. (1945) *Nature (London)* **155,** 24.
21. Epstein, N. (1989) *Chem. Eng. Sci.* **44,** 777–779.
22. Cantor, J. O., Cerreta, J. M., Armand, G. & Turino, G. M. (1997) *Exp. Lung. Res.* **23,** 229–244.
23. Song, Y.-Q., Goodson, B. M., Sheridan, B., de Swiet, T. M. & Pines, A. (1998) *J. Chem. Phys.* **108,** 6233–6239.
24. Mair, R., Cory, D., Peled, S., Tseng, C., Patz, S. & Walsworth, R. (1998) *J. Magn. Reson.* **135,** 478–486.
25. Mair, R. W., Wong, G. P., Hoffmann, D., Hurlimana, M. D., Patz, S. & Schwartz, L. M. (1999) *Phys. Rev. Lett.* **83,** 3324–3327.
26. Rosenthal, F. S. (1999) *J. Appl. Physiol.* **86,** 725–731.
27. Kuwano, K., Matsuba, K., Ikeda, T., Murakami, J., Araki, A., Nishitani, H., Ishida, T., Yasumoto, K. & Shigematsu, N. (1990) *Am. Rev. Respir. Dis.* **141,** 169–178.
28. (1995) *Am. J. Respir. Crit. Care. Med.* **152,** S77–S121.
29. Hautamaki, R. D., Kobayashi, D. K., Senior, R. M. & Shapiro, S. D. (1997) *Science* **277,** 2002–2004.